Supporting Information

Synergistic Effect of Oxygen-Defective $TiNb_2O_7$ Anode and Lithiated Polyacrylic Acid for High-Power Lithium-Ion Storage

Doosoo Kim,[a] Siddhartha Nanda,[a] Jong Heon Kim,[a] Robson S. Monteiro,[b] Luanna Silveira Parreira [b] and Hadi Khani[, a, c]*

[a] Texas Materials Institute and Materials Science and Engineering Program, The University of Texas at Austin, TX 78712, Austin, USA
[b] Companhia Brasileira de Metalurgia e Mineração (CBMM), Gerais 38183903, Brazil
[c] Walker Department of Mechanical Engineering, The University of Texas at Austin, Austin, Texas 78712, USA

* Corresponding author E-mail address: Hadi.Khani@austin.utexas.edu

Table of Content

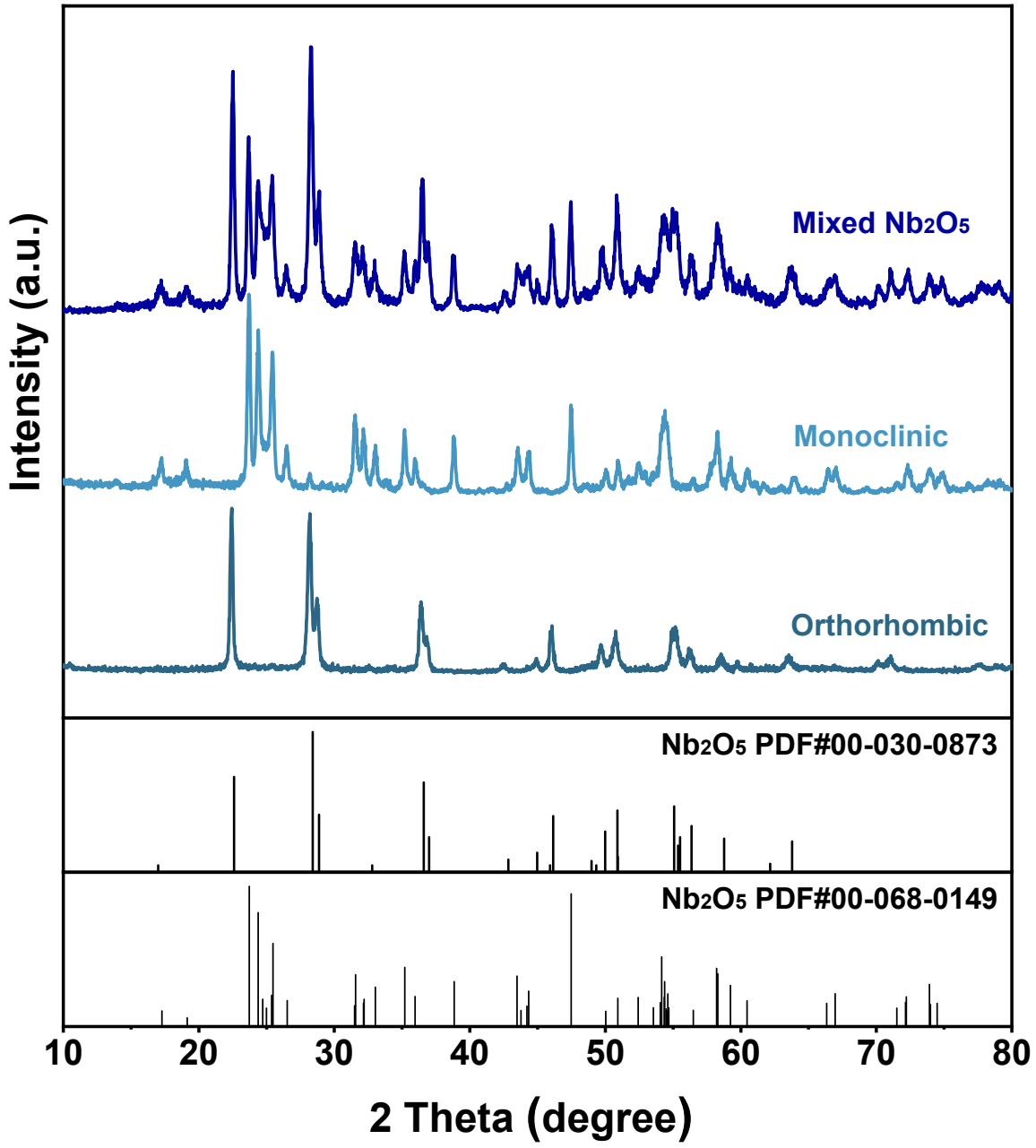

Figure S1. XRD patterns of synthesized Nb_2O_5 with monoclinic, orthorhombic, and mixed monoclinic-orthorhombic phases.

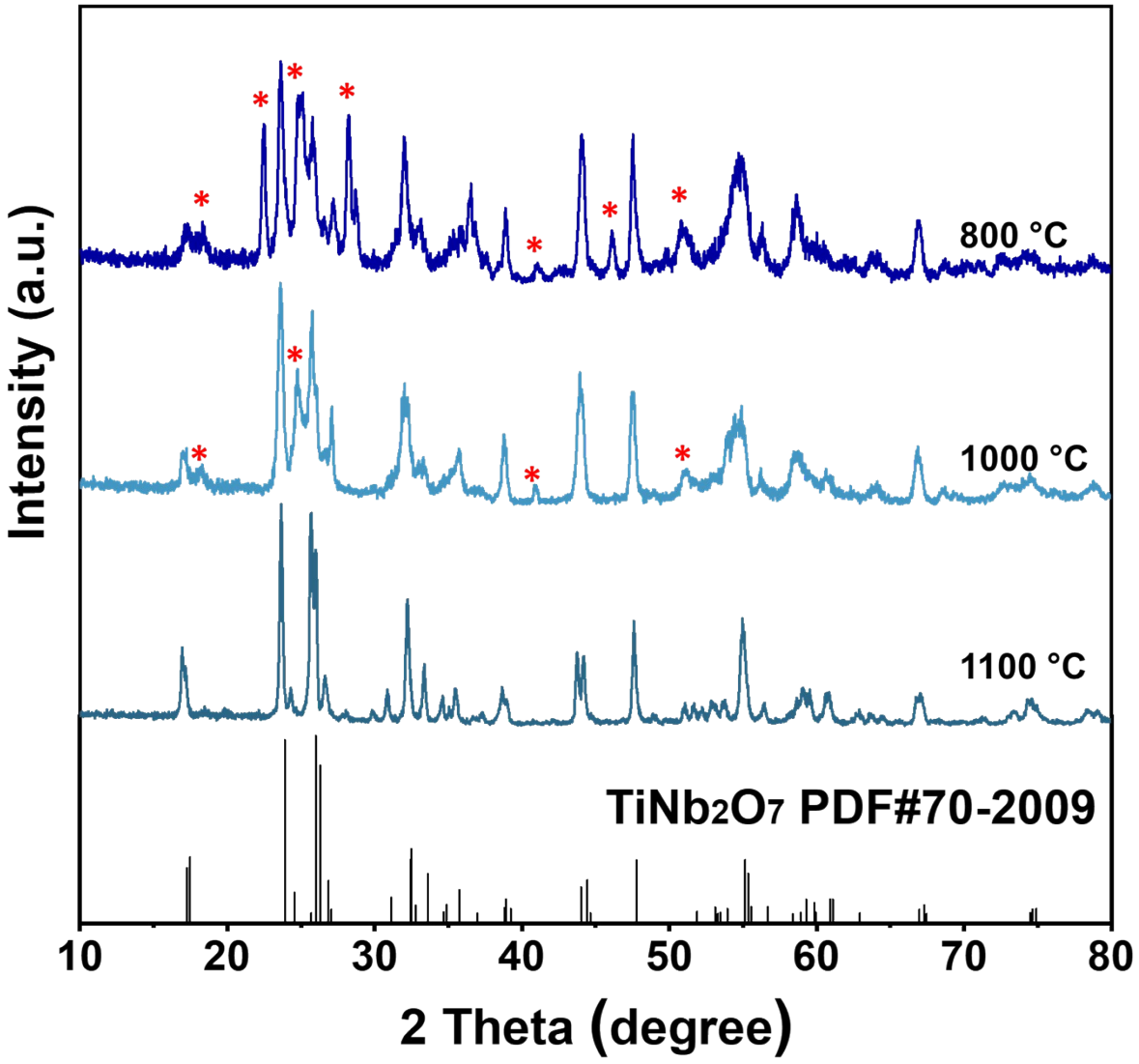

Figure S2. XRD patterns of the $TiNb_2O_7$ synthesized from the orthorhombic Nb_2O_5 precursor at synthesis temperatures of 800, 1000, 1100 ºC, with impurities marked with red asterisks.

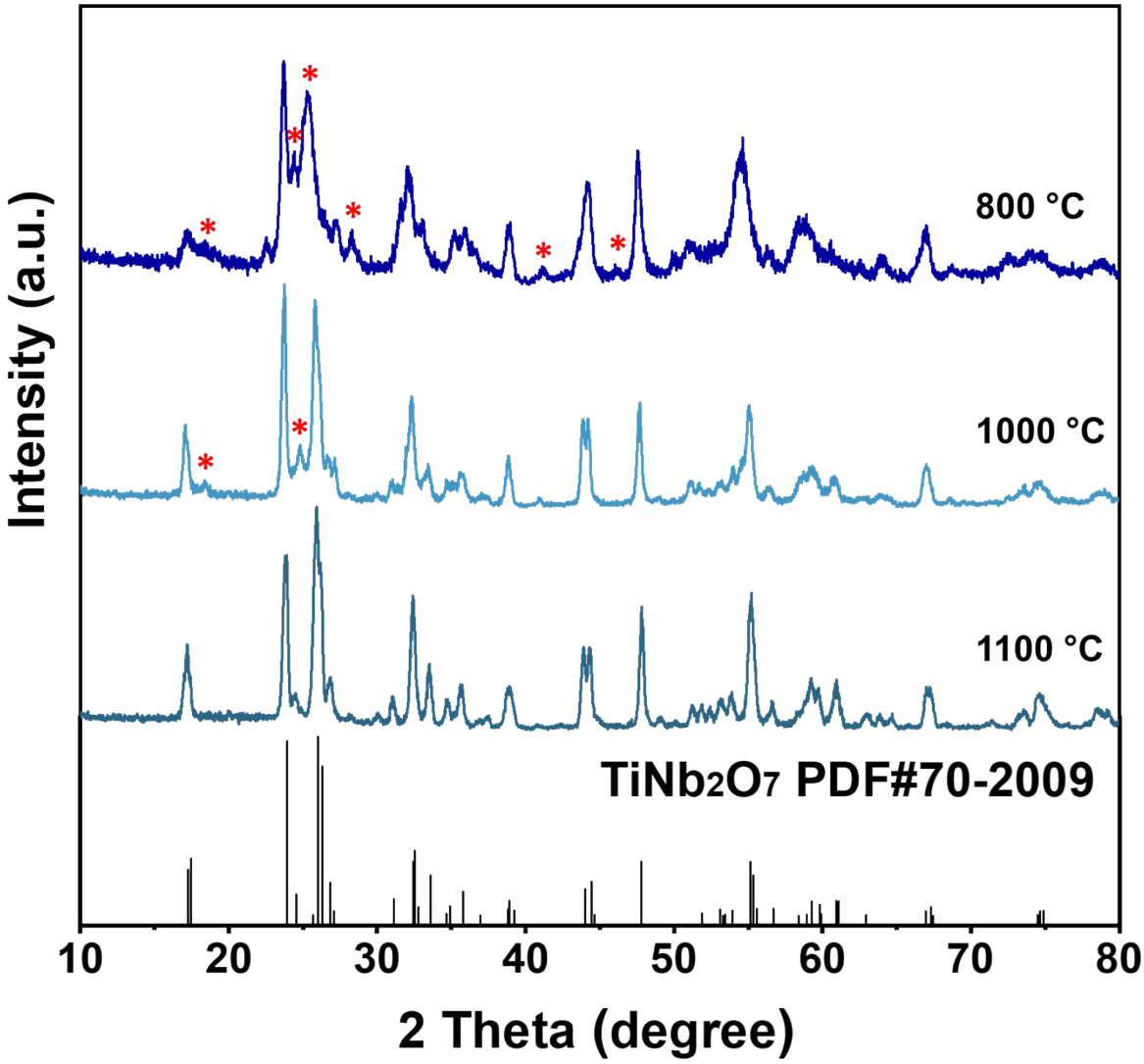

Figure S3. XRD patterns of the $TiNb_2O_7$ synthesized from the monoclinic Nb_2O_5 precursor at synthesis temperatures of 800, 1000, 1100 ºC, with impurities marked with red asterisks.

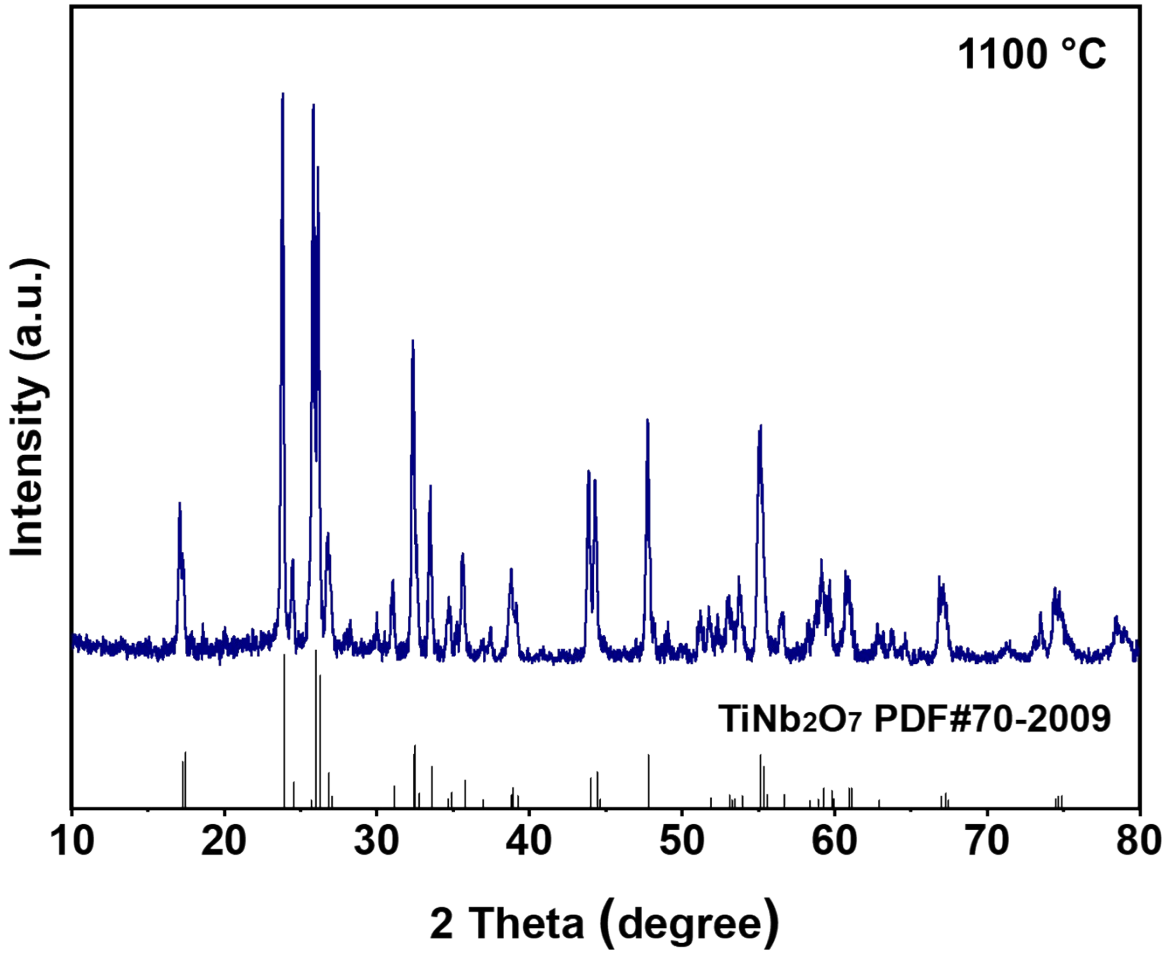

Figure S4. XRD patterns of the $TiNb_2O_7$ synthesized from the Nb_2O_5 precursor with mixed monoclinic-orthorhombic phases at the synthesis temperatures of 1100 ºC.

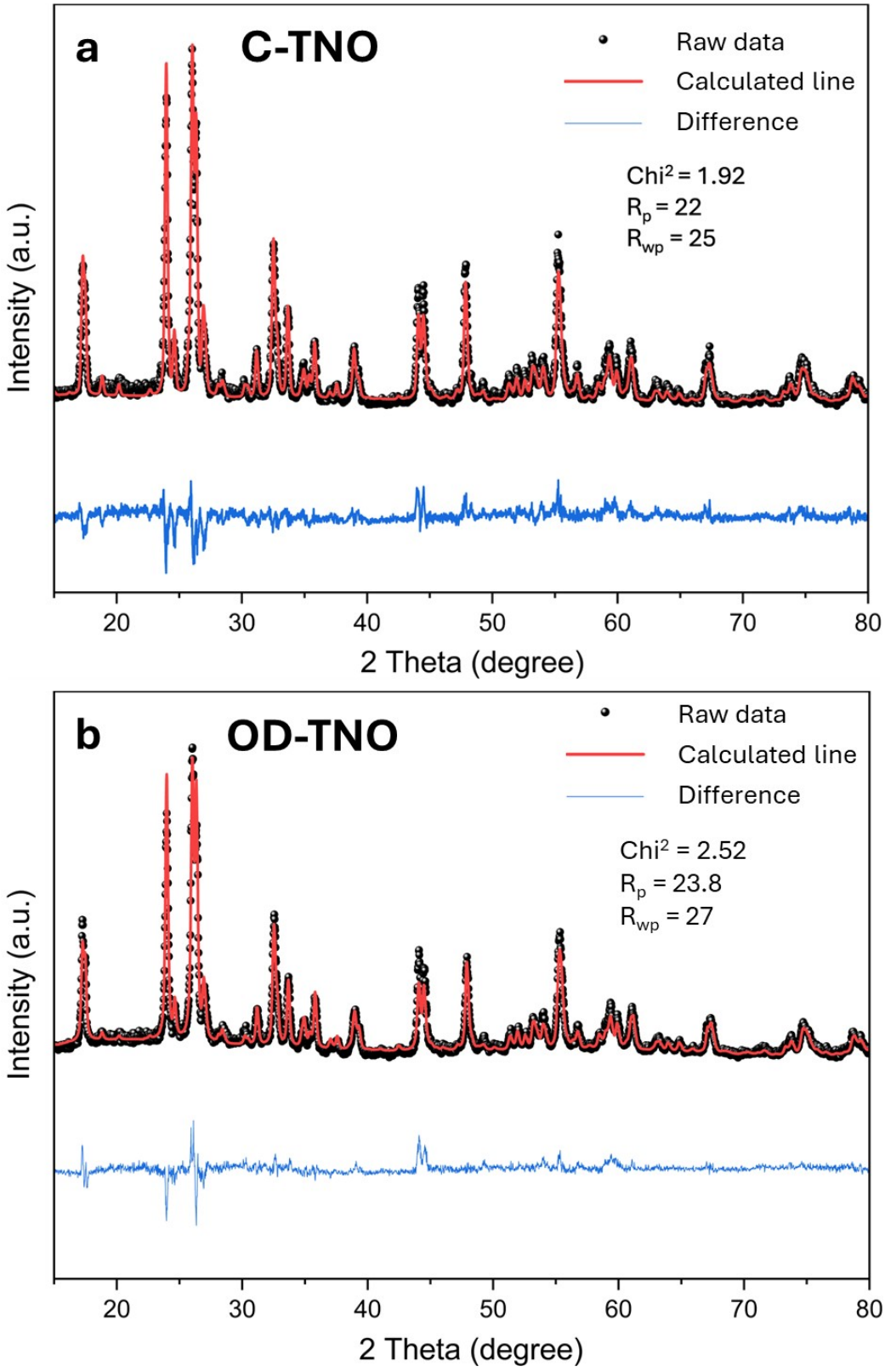

Figure S5. Rietveld refinement of the XRD patterns for C-TNO and OD-TNO.

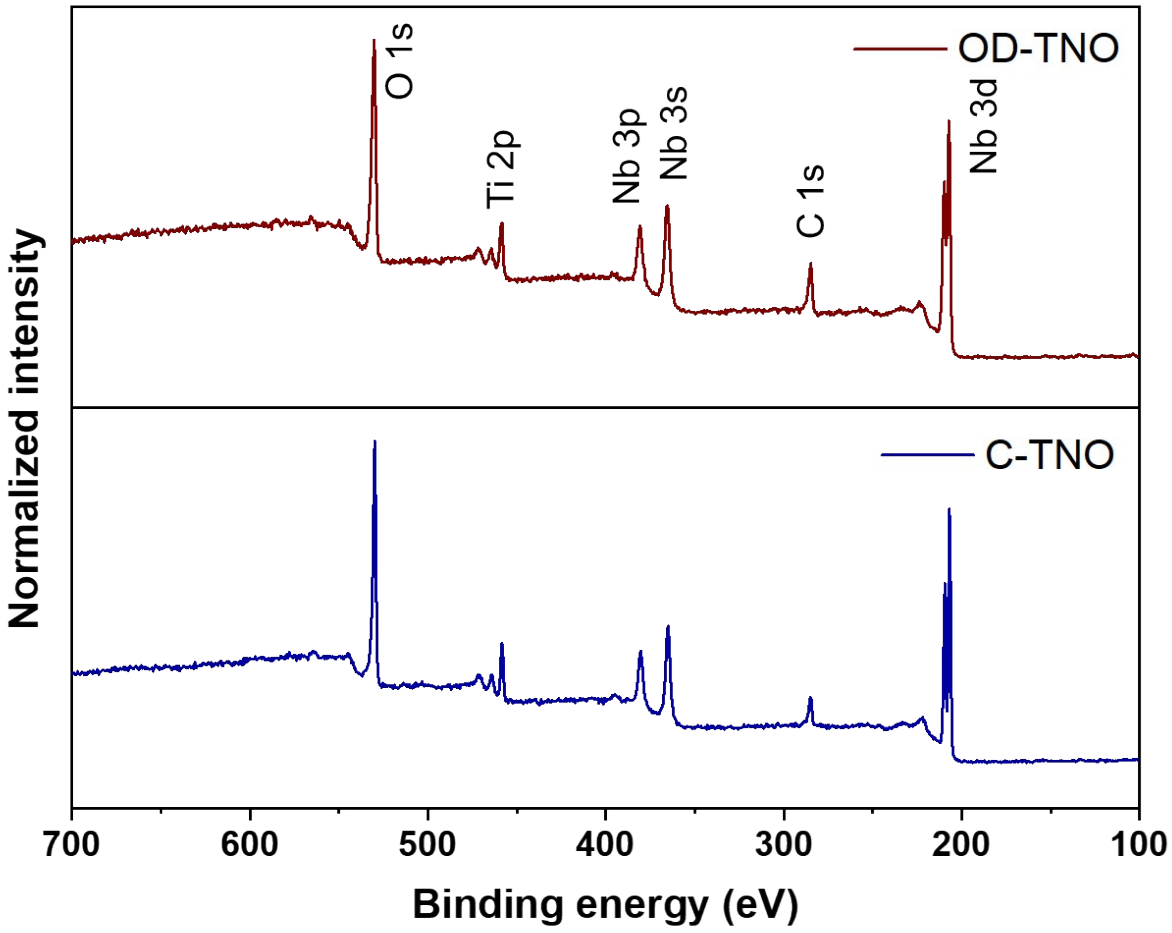

Figure S6. XPS survey spectra of C-TNO and OD-TNO.

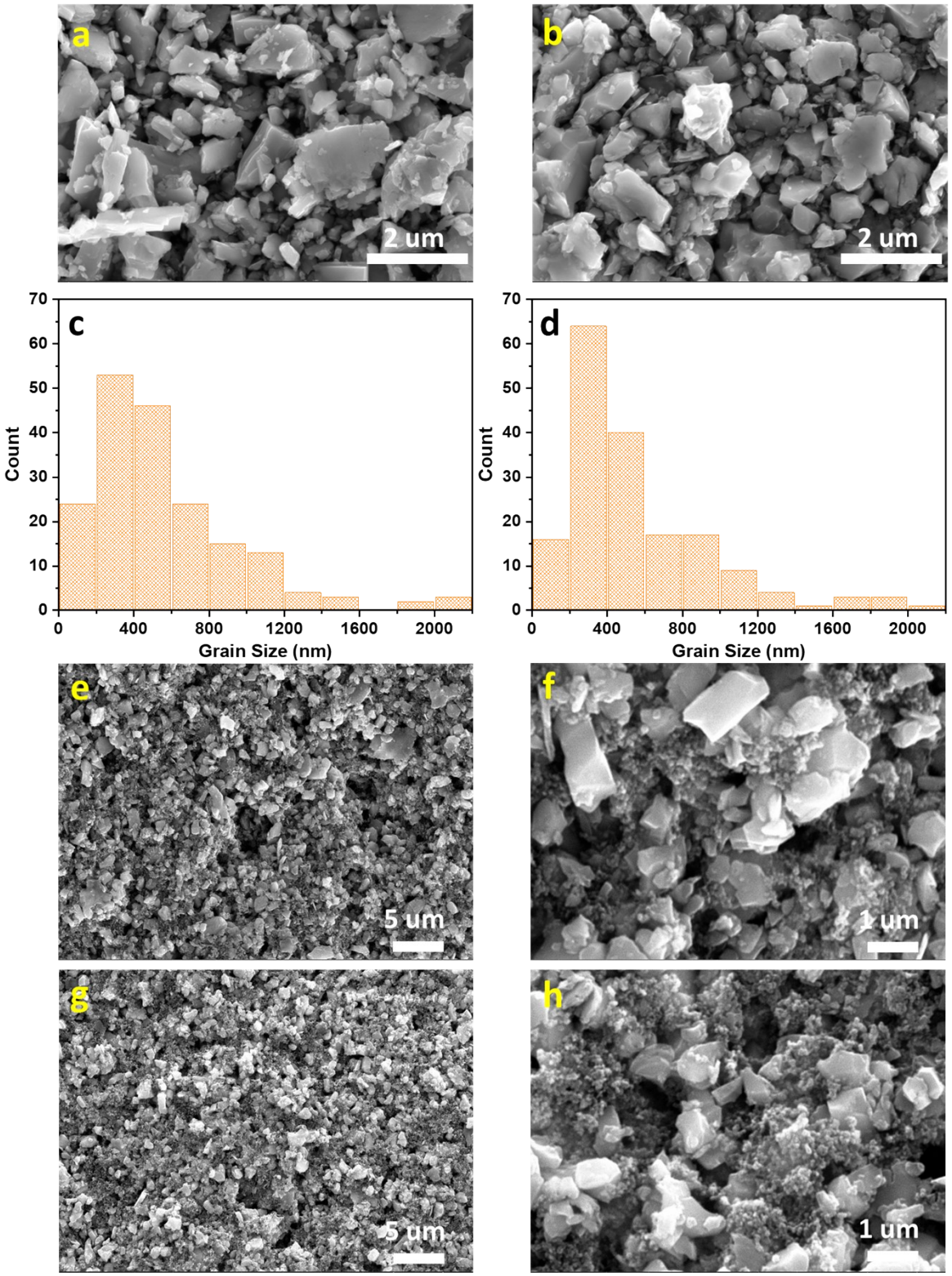

Figure S7. SEM images of ball-milled (a) C-TNO and (b) OD-TNO samples, with their size distribution shown in (c) and (d) respectively. SEM images of (e and f) C-TNO@Super P and (g and h) OD-TNO@Super P.

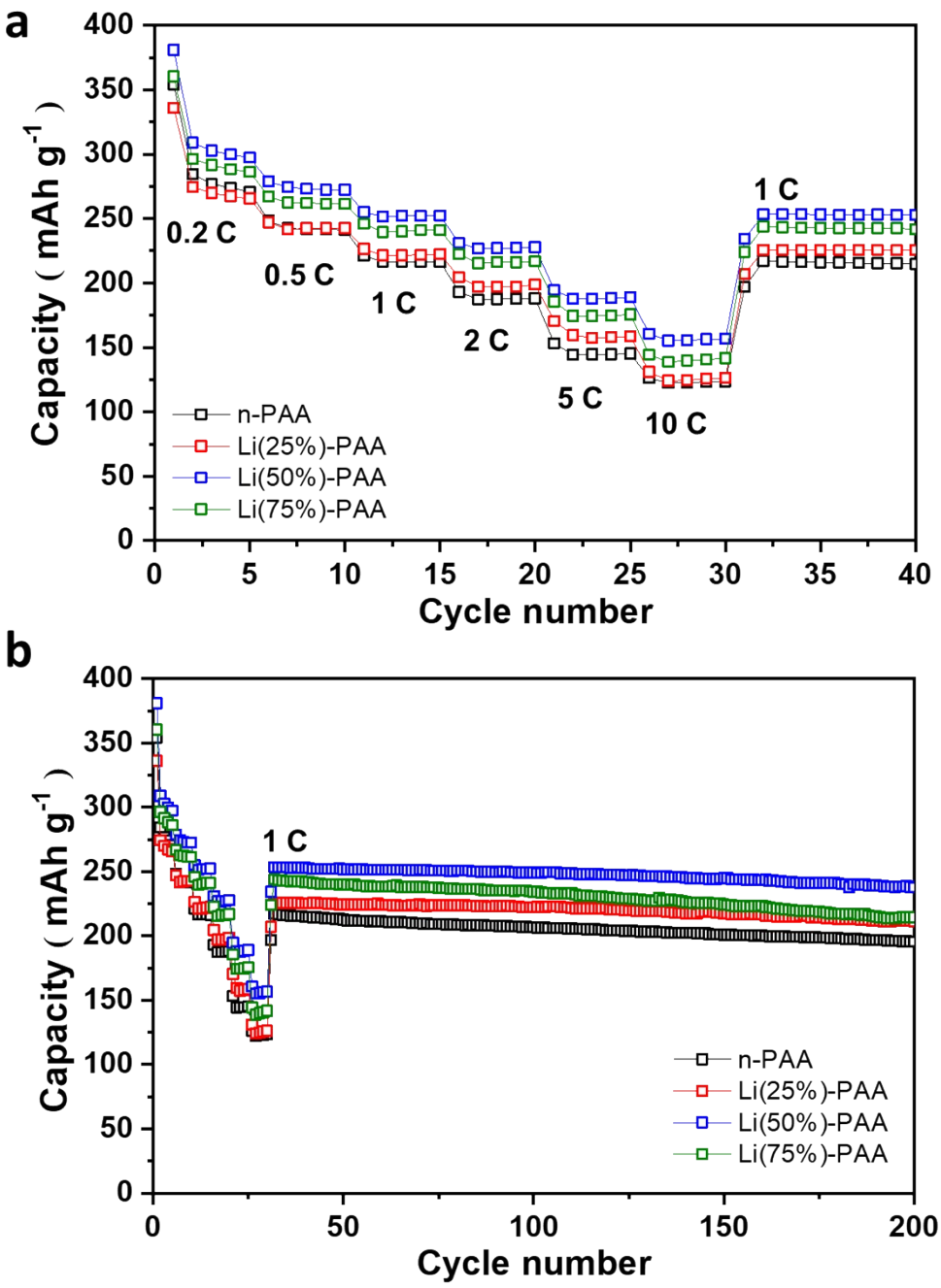

Figure S8. The comparison of (a) rate capability and (b) cycling performance for OD-TNO with different PAA-based binders (PAA, $Li_{25\%}$-PAA, $Li_{50\%}$-PAA, and $Li_{75\%}$-PAA).

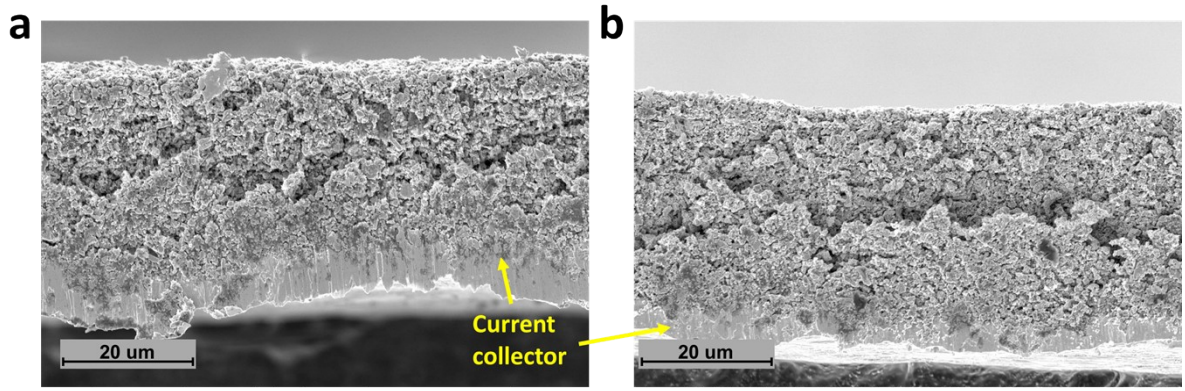

Figure S9. Cross-sectional SEM images of OD-TNO electrodes with (a) PVDF and (b) Li-PAA binders coated on copper current collector.

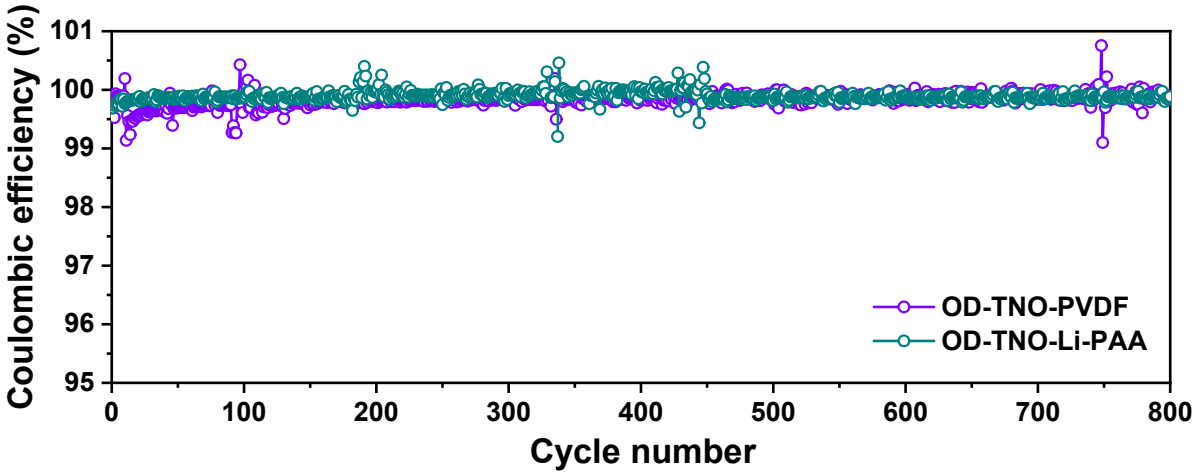

Figure S10. Coulombic efficiency of OD-TNO with PVDF and Li-PAA binders. Cells were subjected to 10 formation cycles that are not shown here.

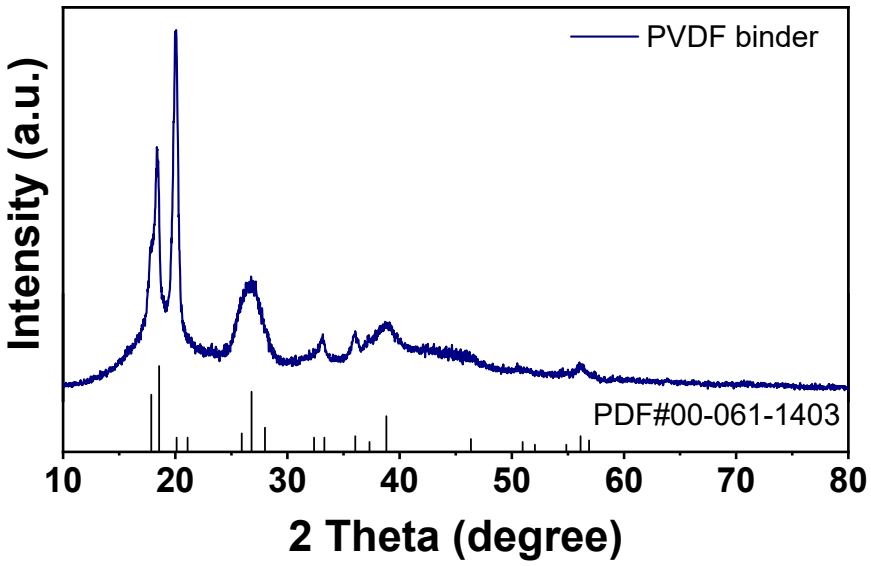

Figure S11. XRD pattern of PVDF binder.

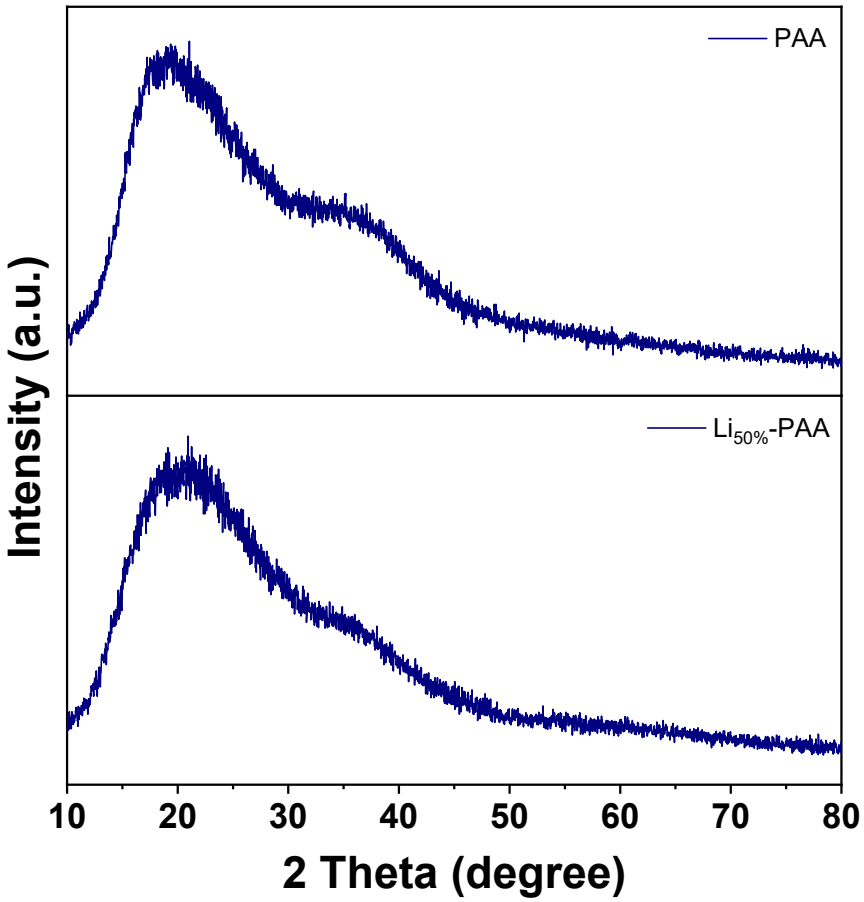

Figure S12. XRD patterns of PAA and $Li_{50\%}$-PAA binders.

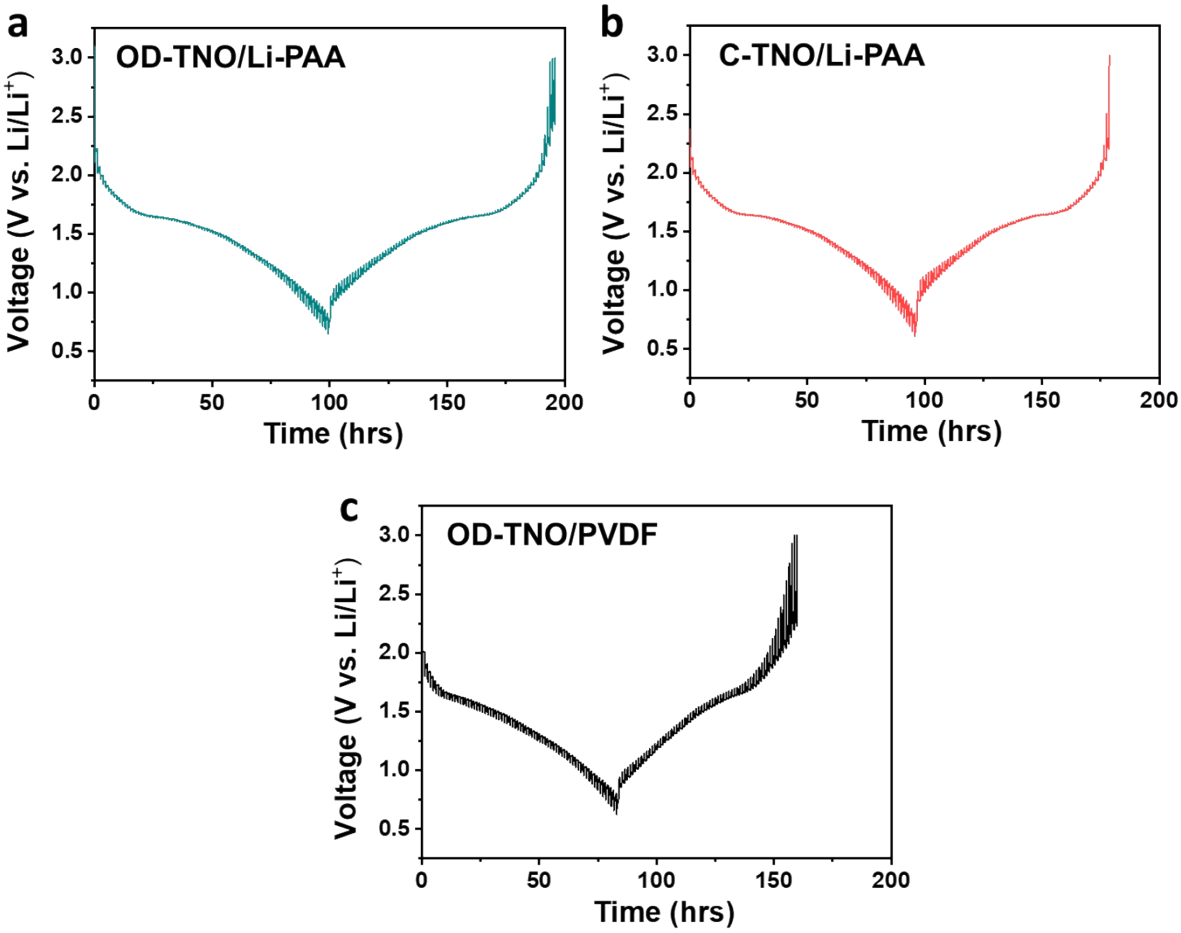

Figure S13. The GITT curves for a) OD-TNO/$Li_{50\%}$-PAA, b) C-TNO/$Li_{50\%}$-PAA, and c) OD-TNO/PVDF.

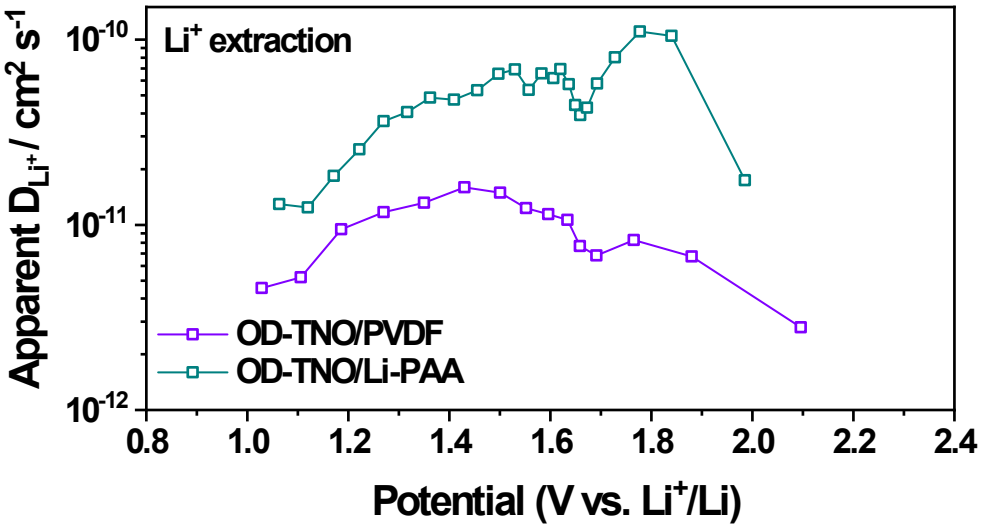

Figure S14. Lithium diffusion coefficients during delithiation process in OD-TNO/PVDF and OD-TNO/Li-PAA.

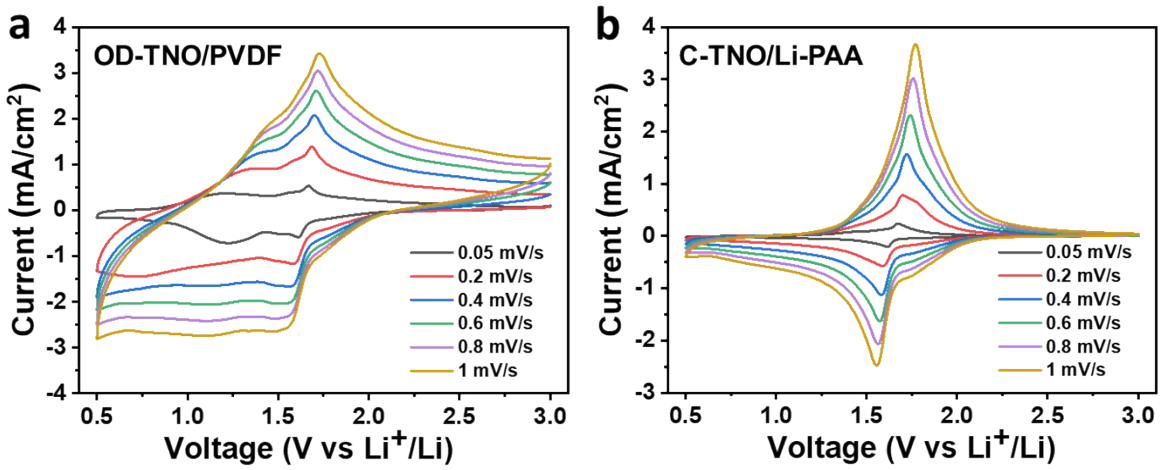

Figure S15. CV curves for a) OD-TNO/PVDF and b) C-TNO/Li-PAA at different scan rates.

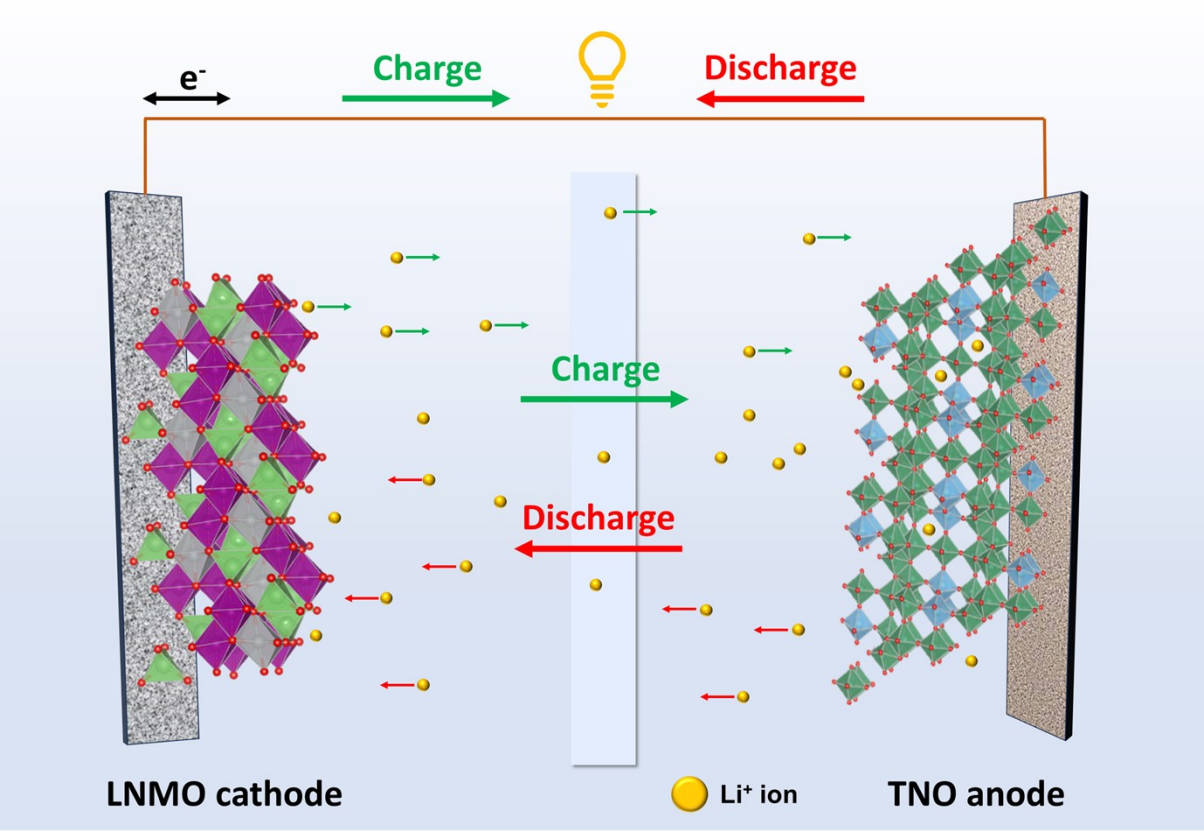

Figure S16. Schematic configuration of $LiNi_{0.5}Mn_{1.5}O_4$//OD-TNO/Li-PAA full cell battery.

Table S1. Comparison of synthesis methods, precursors and experimental times for $TiNb_2O_7$ anode materials in reported literature.

Ref.	Synthesis method	Precursors	Experimental time
[1]	Solid state	TiO_2 and Nb_2O_5	> 96 hours
[2]	Solid state	TiO_2, Nb_2O_5 and Tb_4O_7	24 h
[3]	Solvothermal	Tetrabutyl titanate (TBT), $NbCl_5$, lanthanum acetate (C_6H_9LaO)	24 h (preservation) + 5 h (calcination)
[4]	Solid state	TiO_2, CuO and Nb_2O_5	48h
[5]	Solvothermal	$NbCl_5$, Titanium isopropoxide ($C_{12}H_{28}O_4Ti$)	24 h (autoclave) + 3 h (sintering)
[6]	Solvothermal	Titanium isopropoxide ($C_{12}H_{28}O_4Ti$), niobium ethoxide ($Nb(OC_2H_5)_2$	24 h (autoclave) + 2 h (sintering)
[7]	Sol-gel	Tetrabutyl orthotitanate ($Ti(OC_4H_9)_4$), niobium ethoxide ($Nb(OC_2H_5)_5$)	1 h (stirring) + 3 h (calcination)
[8]	Solvothermal	$NbCl_5$, $Ti(OBu)_4$	16 h (heat treat) + 5 h (annealing)
[9]	Solid state	TiO_2, Nb_2O_5 and Cr_2O_3	20 h
[10]	Solvothermal	Titanium butoxide ($Ti(OC_4H_9)_4$), niobium ethoxide ($Nb(OC_2H_5)_5$)	12 h (autoclave) + 5 h (calcination)
[11]	Solvothermal	Tetrabutyl titanate (TBT), vanadium pentoxide (V_2O_5), $NbCl_5$	24 h (preservation) + 6 h (sintering)
[12]	Solid state	TiO_2, Nb_2O_5, V_2O_5	12 h
[13]	Sol-gel	Nb_2O_5, Nb and TiO_2	24 h
[14]	Solid state	TiO_2 and Nb_2O_5	4 h
[15]	Solvothermal	Niobium ethoxide ($Nb(OC_2H_5)_5$), isopropyl titanate	3 h
[16]	Sol-gel	$NbCl_5$, titanium butoxide	3 h
[17]	Hydrothermal	Titanium isopropoxide ($Ti[OCH(CH_3)_2]_4$), $NbCl_5$, $Cr(CH_3COO)_3$	3 days and 4 h
[18]	Solvothermal	Tetrabutyl titanate (TBT), Ammonium cerium nitrate ($(NH_4)_2Ce(NO_3)_6$), $NbCl_5$	24 h (preservation) + 5 h (sintering)

Table S1 (cont'd). Comparison of synthesis methods, precursors and experimental times for $TiNb_2O_7$ anode materials in reported literature.

Ref.	Synthesis method	Precursors	Experimental time
[19]	Solvothermal	$C_{16}H_{36}O_4Ti$, $C_{10}H_5NbO_{20}$	12 h (stirring) + 1 h (calcination)
[20]	Hydrothermal	$NbCl_5$, titanium isopropoxide	5 h (stirring) + 5 h (calcination)
[21]	Solid state	TiO_2 and Nb_2O_5	15 h

Table S2. Rietveld refinement results for C-TNO and OD-TNO.

Sample	a (Å)	b (Å)	c (Å)	α, γ (°)	β (°)	V (Å^3)
C-TNO	20.361	3.800	11.876	90	120.177	794.334
OD-TNO	20.363	3.797	11.885	90	120.208	794.890

Table S3. Impedance values of OD-TNO with PVDF, PAA and $Li_{50\%}$-PAA binders.

Sample	R_S (Ω)	R_{ct} (Ω)
OD-TNO/PVDF	2.15	96.17
OD-TNO/PAA	2.29	58.46
OD-TNO/$Li_{50\%}$-PAA	2.81	33.94

References

1. K. J. Griffith, I. D. Seymour, M. A. Hope, M. M. Butala, L. K. Lamontagne, M. B. Preefer, C. P. Koçer, G. Henkelman, A. J. Morris and M. J. Cliffe, *Journal of the American Chemical Society*, 2019, **141**, 16706-16725.
2. Y. Zhang, C. Kang, W. Zhao, B. Sun, X. Xiao, H. Huo, Y. Ma, P. Zuo, S. Lou and G. Yin, *Energy Storage Materials*, 2022, **47**, 178–186.
3. K. Tian, Z. Wang, H. Di, H. Wang, Z. Zhang, S. Zhang, R. Wang, L. Zhang, C. Wang and L. Yin, *ACS Applied Materials & Interfaces*, 2022, **14**, 10478-10488.
4. C. Yang, C. Lin, S. Lin, Y. Chen and J. Li, *Journal of Power Sources*, 2016, **328**, 336-344.
5. Y. Zhang, M. Zhang, Y. Liu, H. Zhu, L. Wang, Y. Liu, M. Xue, B. Li and X. Tao, *Electrochimica Acta*, 2020, **330**, 135299.
6. H. Noh and W. Choi, *Journal of The Electrochemical Society*, 2016, **163**, A1042.
7. B. Guo, X. Yu, X.-G. Sun, M. Chi, Z.-A. Qiao, J. Liu, Y.-S. Hu, X.-Q. Yang, J. B. Goodenough and S. Dai, *Energy Environ. Sci.*, 2014, **7**, 2220-2226.
8. Y. Wu, D. Liu, D. Qu, J. Li, Z. Xie, X. Zhang, H. Chen and H. Tang, *Chemical Engineering Journal*, 2022, **438**, 135328.
9. S. Gong, Y. Wang, Q. Zhu, M. Li, Y. Wen, H. Wang, J. Qiu and B. Xu, *J. Power Sources*, 2023, **564**, 232672.
10. H. Park, H. B. Wu, T. Song, X. W. Lou and U. Paik, *Adv. Energy. Mater.*, 2015, **5**, 1401945.
11. K. Liu, J.-a. Wang, J. Yang, D. Zhao, P. Chen, J. Man, X. Yu, Z. Wen and J. Sun, *Chemical Engineering Journal*, 2021, **407**, 127190.
12. X. Wen, C. Ma, C. Du, J. Liu, X. Zhang, D. Qu and Z. Tang, *Electrochimica Acta*, 2015, **186**, 58-63.

13. J.-T. Han, Y.-H. Huang and J. B. Goodenough, *Chemistry of Materials*, 2011, **23**, 2027-2029.

14. N. V. Kosova, D. Z. Tsydypylov, E. S. Papulovskiy and O. B. Lapina, *The Journal of Physical Chemistry C*, 2022, **126**, 13607-13616.

15. R. Qian, H. Lu, T. Yao, F. Xiao, J.-W. Shi, Y. Cheng and H. Wang, *ACS Sustainable Chemistry & Engineering*, 2021, **10**, 61-70.

16. H. Lyu, J. Li, T. Wang, B. P. Thapaliya, S. Men, C. J. Jafta, R. Tao, X.-G. Sun and S. Dai, *ACS Applied Energy Materials*, 2020, **3**, 5657-5665.

17. Y.-S. Hsiao, L.-Y. Chang, C.-W. Hu, C.-Z. Lu, N.-J. Wu, Y.-L. Chen, T.-H. Hsieh, J.-H. Huang, S.-C. Hsu and H.-C. Weng, *Applied Surface Science*, 2023, **614**, 156155.

18. A. Shi, Y. Zhang, S. Geng, X. Song, G. Yin, S. Lou and L. Tan, *Nano Energy*, 2024, **123**, 109349.

19. W. Zhu, B. Zou, C. Zhang, D. H. Ng, S. A. El-Khodary, X. Liu, G. Li, J. Qiu, Y. Zhao and S. Yang, *Advanced Materials Interfaces*, 2020, **7**, 2000705.

20. H. Choi, T. Kim and H. Park, *Electrochimica Acta*, 2022, **404**, 139603.

21. A. A. Voskanyan, K. Jayanthi and A. Navrotsky, *Chemistry of Materials*, 2022, **34**, 10311-10319.